Available online at www.sciencedirect.com
SCIENCE DIRECT
Journal of Catalysis 227 (2004) 530–536
JOURNAL OF CATALYSIS
www.elsevier.com/locate/jcat

Morphology of WS_2 nanoclusters in WS_2/C hydrodesulfurization catalysts revealed by high-angle annular dark-field scanning transmission electron microscopy (HAADF-STEM) imaging

Anna Carlsson *, Michael Brorson, Henrik Topsøe

Haldor Topsøe A/S, Nymøllevej 55, DK-2800 Lyngby, Denmark

Received 7 June 2004; revised 17 August 2004; accepted 19 August 2004

Available online 17 September 2004

Abstract

Tungsten disulfide (WS_2) nanoclusters supported on high surface area graphite are studied by use of high-angle annular dark-field scanning transmission electron microscopy (HAADF-STEM) imaging. It is found that HAADF-STEM, in contrast to high-resolution transmission electron microscopy (HRTEM), enables ready observation of all the WS_2 nanoclusters and gives direct insight into their morphology. Such measurements may thus provide a more detailed and quantitative basis for establishing activity correlations. The S–W–S layers of the WS_2 nanocluster structure are found to be oriented parallel to the graphite surface and with an apparent topotactic orientation relationship. Whereas many WS_2 nanoclusters are observed to be irregular in shape, hexagonal and more often triangular or truncated triangular shapes are also encountered. The shape variations within a particular sample are larger than the shape variations between different samples each prepared by a particular sulfiding procedure. The vast majority of nanoclusters contains only a single S–W–S layer even after sulfiding at 1073 K.

Keywords: HAADF-STEM; HRTEM; Hydrodesulfurization; HDS; WS_2; Morphology; Carbon; Graphite; Support interaction

1. Introduction

Molybdenum- and tungsten-based catalysts promoted with cobalt or nickel have been used extensively in refineries to remove sulfur from different oil fractions [1–3]. With the recent emphasis on the production of ultralow sulfur transport fuels [4–7], there is a renewed interest in understanding the detailed structure of such hydrodesulfurization (HDS) catalysts.

HDS catalysts have been the subject of numerous characterization studies [2], and today there is general agreement that after sulfiding Mo (W) is present as MoS_2 (WS_2), which has a characteristic structure consisting of S–Mo–S (S–W–S) layers. Many structure–activity correlation studies of these highly anisotropic systems suggest that the catalysis is related to the sites along the edges of the individual S–Mo–S (S–W–S) layers [2]. This is also the location where the promoter atoms are found in the so-called Co–Mo–S (Ni–Mo–S, Co–W–S, and Ni–W–S)-type structures [2]. In view of the importance of the edge sites, there has been a particular interest in obtaining information about the edge dispersion and a detailed morphology of the MoS_2 (WS_2) nanoclusters. The latter type of information is highly relevant if we are to gain more detailed insight and address the role of edges and corner sites. In typical supported HDS catalysts such insight has been difficult to obtain since the MoS_2 (WS_2) material consists of very small ($\leqslant 2$ nm), X-ray amorphous clusters. The identity of these clusters was first established by EXAFS [8] and since then this technique has provided further valuable insight [9–16]. EXAFS experiments may, for example, be used to estimate the edge dispersion of the MoS_2 (WS_2) nanoclusters. However, disorder and surface reconstruction effects make such measurements quite inaccurate and EXAFS typically overestimates the edge dispersion [2,9,14–16]. Also, EXAFS experiments do not allow a detailed

* Corresponding author.
E-mail address: abc@topsoe.dk (A. Carlsson).

0021-9517/$ – see front matter
doi:10.1016/j.jcat.2004.08.031

insight into the 3D structures of the nanoclusters. Early FTIR and XPS studies showed that single-layer MoS_2 sheets dominate under mild sulfiding conditions [17,18]. However, the key techniques for providing insight into the morphology of the MoS_2 (WS_2) nanoclusters have been high-resolution electron microscopy (HRTEM) [19–38]. In such experiments the individual S–Mo–S layers of the MoS_2 structure may be imaged and their number and projected length in each MoS_2 nanocluster may be determined. From measurements of a large number of nanoclusters, estimates of the edge dispersion [22,30,33,34] may be obtained and valuable insight into the effects of sulfiding and changing catalyst compositions may be gained. Such measurements have also been the basis for interesting activity correlations [34].

There are also several problems associated with the application of HRTEM. For example, several HRTEM experiments [22,30,32] suggest that HRTEM will not image the very smallest nanoclusters (e.g., those containing less than about 7 Mo atoms). For some catalysts, this may constitute the majority of the nanoclusters. However, it has been shown that nanometer-sized spherical oxysulfide or sulfide particles can be observed on samples that have not been exposed to air [37,38]. These particles show very low contrast in HRTEM images of practical catalysts and are usually only observed in profile view on the edges of the support particles. Another problem with the application of HRTEM to supported catalysts is that not all orientations with respect to the electron beam of the highly anisotropic, layered MoS_2 (WS_2) structure will be imaged. The layers are viewed as lines when imaged perpendicular to the c axis, and typically atomic images are obtained only when imaging along the ⟨100⟩ and ⟨110⟩ directions [32]. Since images are not obtained along the c axis, no information about the shape/morphology of the layers is obtained. Thus in order to arrive at estimates of the concentration of edge sites, corner sites, etc., one has had to rely on assumptions regarding the MoS_2 (WS_2) nanocluster morphology. Typically, the hexagonal morphology was assumed. Recently, it was possible to support small MoS_2 nanoclusters on Au(111) single crystal surfaces and to characterize their structure and morphology in detail by use of scanning tunneling microscopy (STM) [39,40]. These studies show that MoS_2 nanoclusters may also exhibit non-hexagonal morphology. With this background, it is highly desirable to obtain detailed morphological insight into supported catalyst systems that are closer to the industrial catalysts, i.e., where the support and preparation parameters may play key roles in determining their structure [2].

Presently we will show that WS_2 nanocluster morphology information can be obtained from high surface area supported catalysts by use of high-angle annular dark-field scanning transmission electron microscopy (HAADF-STEM) imaging. This technique was first applied in dedicated STEM instruments and uses the electrons scattered at high angles to create a Z-contrast image [41–45]. Today, more readily available combined TEM-STEM instruments are commonly used. It has been shown that it is possible to use HAADF-STEM to detect single heavy atoms on a light support. If a small enough probe can be formed, HAADF-STEM also gives the possibility for atomic resolution Z-contrast imaging. Scattering is caused by the nucleus and follows roughly a Z^2 dependence. We therefore use a heavy element sulfide, WS_2, on a light element support, carbon. In such carbon-supported catalysts, the support interactions are expected to be quite weak and the catalytic properties resemble those of the high activity Type II structures [2].

2. Experimental

2.1. Sample preparation

Graphitic carbon (Timcal Timrex HSAG100 CAT, Special Graphite, M-292) with a BET surface area of 118 m^2/g is used as support. The carbon powder was tabletized, granulated, impregnated by the incipient wetness method with an aqueous solution of ammonium metatungstate, and dried in air at 110 °C. The tungsten loading was determined to be approximately 0.6 wt%. The sample was split in three parts, placed in quarts boats, and sulfided in a tube furnace under different conditions. The samples were sulfided as follows: $WS_2/C(H_2S/H_2)$, 10% H_2S in H_2 for 6 h at 1073 K and then cooling to room temperature in N_2; $WS_2/C(H_2S/H_2, H_2)$, 10% H_2S in H_2 for 6 h at 1073 K and then 100% H_2 for 4 h at 673 K, and finally cooling to room temperature in N_2; $WS_2/C(H_2S)$, 100% H_2S for 6 h at 1073 K and then cooling to room temperature in N_2. All samples were passivated by means of 1% O_2 in N_2 before they were quickly transferred from the cold tube furnace to a container where they were stored under N_2 until TEM analysis.

2.2. Microscopy

The samples were crushed in a mortar and deposited dry on standard Cu TEM grids covered with lacey carbon. Both TEM and HAADF-STEM measurements were performed on a Philips CM200 FEG UltraTwin electron microscope, with a primary electron energy of 200 keV, $C_s = 0.5$ mm, and a point-to-point resolution of 1.9 Å in TEM mode. The resolution in STEM mode depends on the instrument settings used, but the images presented here have a resolution of ca. 0.4 nm, as determined from the observation of lattice fringes. The alignment for STEM was carried out using ronchigrams [46]. The contrast in HAADF images is approximately proportional to $Z^{1.7}$ [45], and this is thus an excellent technique for observing heavy nanoparticles (e.g., WS_2) on a light support (e.g., C). In contrast to HRTEM, quantitative analysis of images is quite straightforward. EDS spectra were recorded with an EDAX spectrometer using a probe size of around 5 nm.

3. Results and discussion

The graphite support has a flake-like structure with a typical flake thickness of 5–10 nm. When HRTEM images of the sulfided catalysts are obtained with the electron beam *parallel* to a graphite sheet (i.e., edge on), S–W–S layers can be viewed as lines. This is in complete analogy with previous TEM investigations of supported Mo or W catalysts (see, e.g., [22,23,32,33]) and these results are not given here. However, they do show that the WS_2 sheets are attached flatly onto the graphite surface. Fig. 1 shows HRTEM and HAADF-STEM images of the same WS_2 nanocluster imaged with the electron beam *perpendicular* to the graphite sheet. The contrast in the HRTEM image is weak and direct observation of the WS_2 nanoclusters is difficult. Thus, with the present samples we encounter the same problems that previous investigations identified [32,33], and HRTEM is not suitable to provide detailed information about the shape of the WS_2 nanoclusters. In the Fourier transform peaks corresponding to WS_2 can be distinguished, in addition to the peaks stemming from the graphite support. Fourier filtering using the WS_2 peaks can give an indication of the location and general shape of the WS_2 nanoclusters, but a detailed analysis of the shape is not possible from such filtered images. The same area imaged with HAADF-STEM shows excellent contrast and the morphology of the WS_2 nanocluster can be studied in detail. The Fourier transform also shows a near parallel orientation of the graphite and WS_2 lattices, indicating a topotactic relationship.

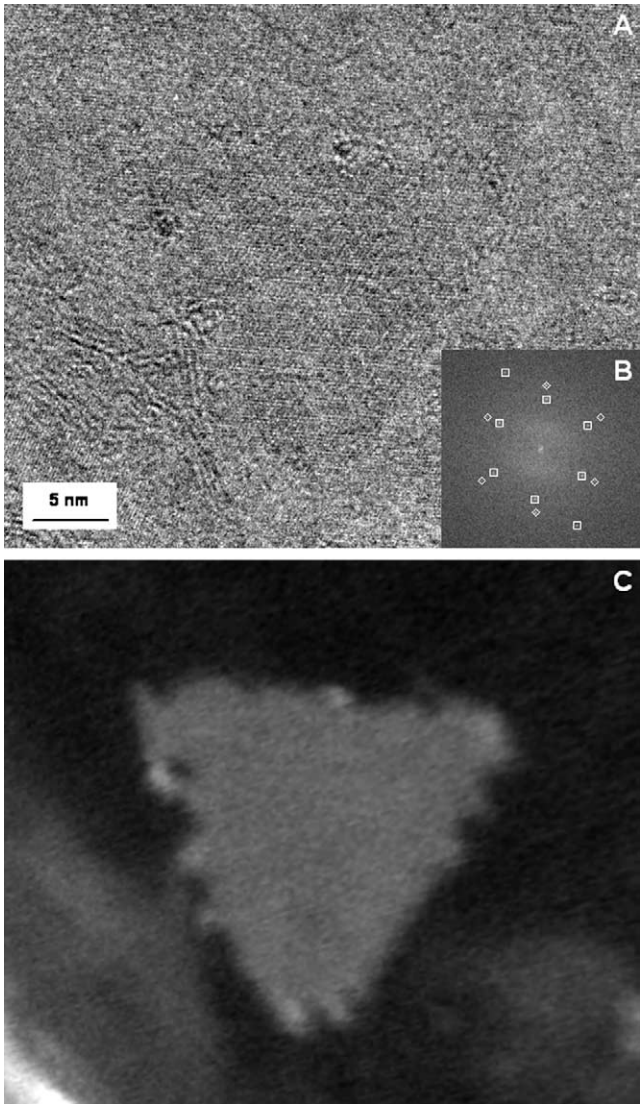

Fig. 1. HRTEM (A) and HAADF-STEM (C) images of the same WS_2 nanocluster. In the HRTEM image the contrast is very weak and the exact shape of the WS_2 nanocluster is difficult to discern. The Fourier transform (B) of the HRTEM image shows peaks corresponding to graphite (◇) and WS_2 (□). The particular sample imaged is $WS_2/C(H_2S/H_2, H_2)$.

Fig. 2 shows an example of an HAADF-STEM image that has been obtained with the electron beam *perpendicular* to a graphite sheet. Many bright structures with regular shapes (ca. 1–100 nm in diameter) ranging from triangular to hexagonal are readily observed (Fig. 3), but it is noteworthy that many of the structures are quite irregular. In view of the quite large difference in contrast between the bright structures and the background, it is likely that the structures originate from WS_2 nanoclusters. This is confirmed by performing energy dispersive spectroscopy (EDS) on the bright areas and comparing the result with that of the adjacent graphite background (Fig. 4). The EDS measurements were performed with a stationary, defocused probe (ca. 5 nm), and no beam damage was visible in the image after spectrum recording. Besides the clear presence of W in the bright areas, the EDS

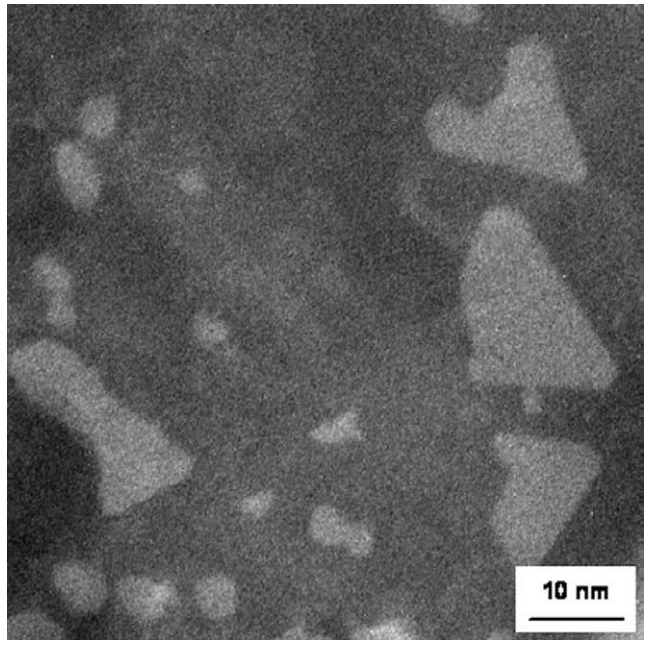

Fig. 2. HAADF-STEM image of several WS_2 nanoclusters supported on a graphite sheet. In contrast to HRTEM, the shape of even very small structures (< 3 nm) can be clearly discerned in the HAADF-STEM image. While many WS_2 nanoclusters are irregular, triangular and hexagonally shaped nanoclusters are also clearly visible. The particular sample imaged is $WS_2/C(H_2S/H_2, H_2)$.

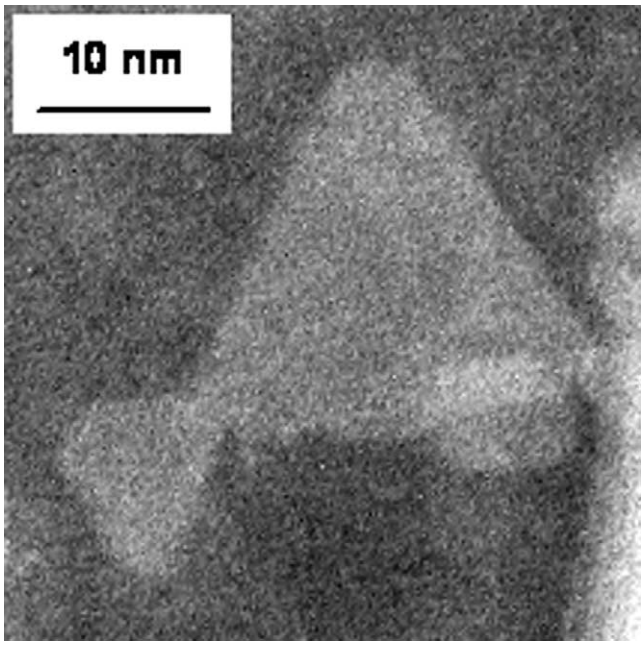

Fig. 3. HAADF-STEM image of two regularly shaped, truncated WS_2 triangles. It is unclear whether the two structures are located on the same side of the graphite sheet, but in any case their similar orientations could indicate a topotactic relationship to the support. The particular sample imaged is $WS_2/C(H_2S/H_2)$.

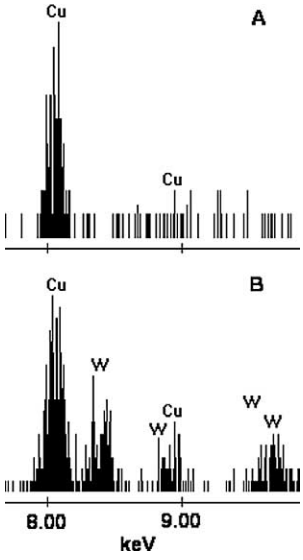

Fig. 4. EDS analysis of the graphite support (A) and a supported WS_2 nanocluster (B). Note the complete lack of W signal in A. The EDS spectrum denoted B was recorded with the probe centered on a single-layer WS_2 slab, whereas the one denoted A was recorded with the edge of the probe a few nanometers away from the slab. The Cu signal originates from the TEM grids. The particular EDS analysis shown was made on the sample $WS_2/C(H_2S/H_2)$.

spectrum also shows, at low energies, the presence of sulfur. No attempts at quantitative analysis of the spectra were made due to the low number of counts.

The quite uniform intensity of the areas in the images where WS_2 nanoclusters are present indicates that the nanoclusters almost all have the same thickness. Several observations, to be discussed in the following, together evidence that most WS_2 nanoclusters are monolayer structures, i.e., that they consist of only a single S–W–S sheet. One observation is that the nanoclusters in typical HAADF-STEM images were found to cover approximately 6% of the graphite sheets. This value agrees quite well with the calculated coverage of 4% assuming that all WS_2 is present as monolayer structures and that all graphite sheets have a thickness of 10 nm. It should be noted that in the images we may observe WS_2 nanoclusters that are located on the same graphite sheet both on top and underneath. In some images (Fig. 5) we even observe accidentally overlapping WS_2 nanoclusters located on top and underneath a particular graphite sheet. A nice feature of HAADF-STEM is that quantitative analysis is performed in a straightforward manner. If we use the $Z^{1.7}$ dependence of the intensity and the typical thickness of the graphite sheets, the observed intensity difference between the WS_2 structures and the graphite support also agrees well with the predominance of monolayer WS_2 nanoclusters. The same conclusion is arrived at when the lacey carbon support is used as an internal scattering standard. Finally, when the graphite sheets are imaged edge on (Fig. 6), we almost exclusively observe single-layer WS_2 sheets.

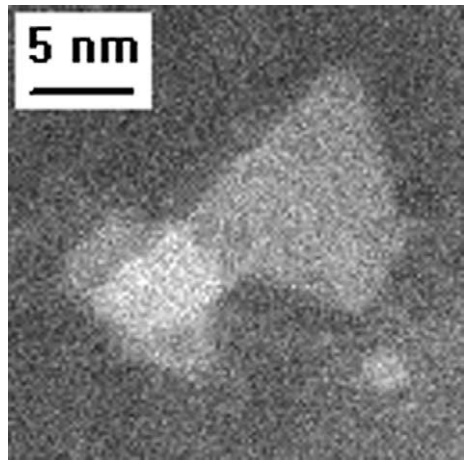

Fig. 5. HAADF-STEM image of a composite structure that most likely arises from accidental overlap of WS_2 nanoclusters located on opposite sides of the graphite sheet. The particular sample imaged is $WS_2/C(H_2S/H_2, H_2)$.

All the above HAADF-STEM results show that the WS_2 nanoclusters are attached flatly onto the graphite surfaces. Quite often it is observed that adjacent WS_2 nanoclusters are oriented in the same way. This indicates a quite strong topotactic interaction with the support. The dominating occurrence of monolayer structures, even after sulfiding at 1073 K, also supports this and it is therefore likely that the interaction energy with the graphite support is greater than that existing between S–W–S layers of WS_2. The apparent topotactic behavior may also be related to the observation that the WS_2 nanoclusters may preferentially be located at graphite step edges (Fig. 7). The irregular shapes may be re-

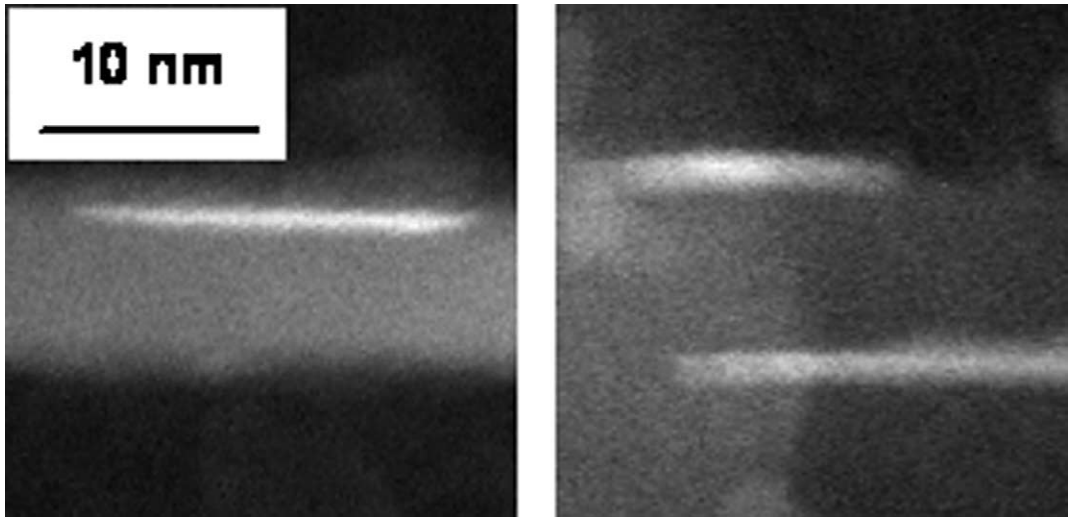

Fig. 6. HAADF-STEM images of graphite sheets imaged edge on. Note the presence of single-layer WS_2 nanoclusters on one or both sides of the sheets. The particular sample imaged is $WS_2/C(H_2S/H_2, H_2)$.

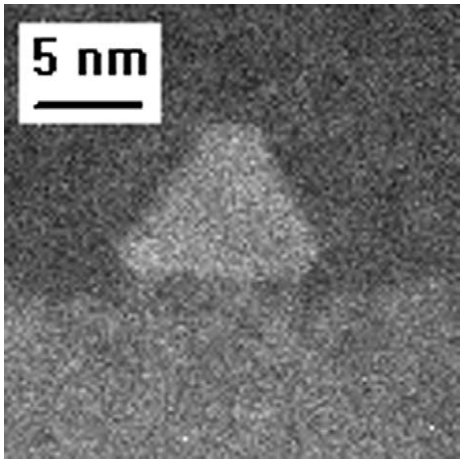

Fig. 7. HAADF-STEM image of a WS_2 nanocluster shaped as a regular truncated triangle. Note that one edge of the nanocluster follows a step on the graphite surface. The particular sample imaged is $WS_2/C(H_2S/H_2, H_2)$.

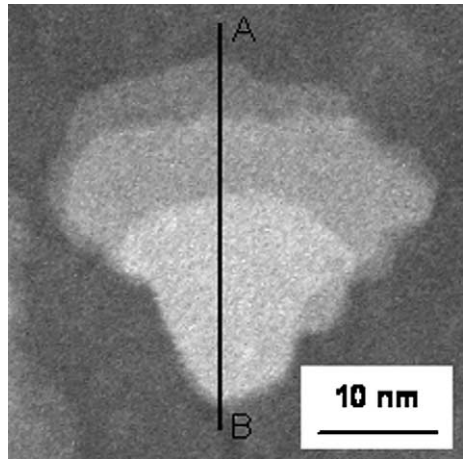

Fig. 8. HAADF-STEM image of a very irregular, multilayer WS_2 nanocluster. The shape seems to be determined by a structure on the graphite surface. As quantified in Fig. 9, the varying intensity in the nanocluster image is due to different number of S–W–S layers in different parts of the cluster. Thus in the brightest part the cluster contains 3 S–W–S layers. The particular sample imaged is $WS_2/C(H_2S)$.

lated to growth starting from irregular graphite steps. It is also likely that during the growth process, WS_2 islands will meet new step edges that will halt the growth in this direction and influence the final shape.

In some cases, the apparent multilayer structures are, as discussed above, the result of the overlap between images of WS_2 nanoclusters located at opposite sides of the graphite sheet. In other areas, the multilayer structures are clearly associated with the same particle (Fig. 8). The intensity analysis taken across the particle (Fig. 9) shows that the intensity increases in steps corresponding to one S–W–S layer.

Previous catalytic measurements showed that the properties of HDS catalysts depend on the choice of sulfiding procedure (see, e.g., [2]). Recent DFT calculations [47–53] and STM observations [39,40] have provided a basis for understanding such phenomena since the tendency for exposing the $(10\bar{1}0)$ Mo and $(\bar{1}010)$ S edges depends on the chemical potential of the gaseous environment of MoS_2. Thus, highly sulfiding conditions will favor the formation of the Mo edges [40,48,52] and MoS_2 triangles exposing only these edges can in fact be observed [39,40]. Under more reducing conditions, truncated MoS_2 triangles or hexagons exposing both types of edges were observed [40]. In view of the prior calculations and STM observations on model systems, the effect of different sulfiding treatments was also investigated in the present study. For the WS_2/C catalysts studied here, the morphological effects appear much more complex than those observed by STM on MoS_2/Au. The WS_2/C catalysts display much larger shape variations within each individual sample than between the three samples that had been obtained by means of different sulfiding gas mixtures. It will in fact require a statistical analysis of many WS_2/C images before detailed conclusions regarding the ef-

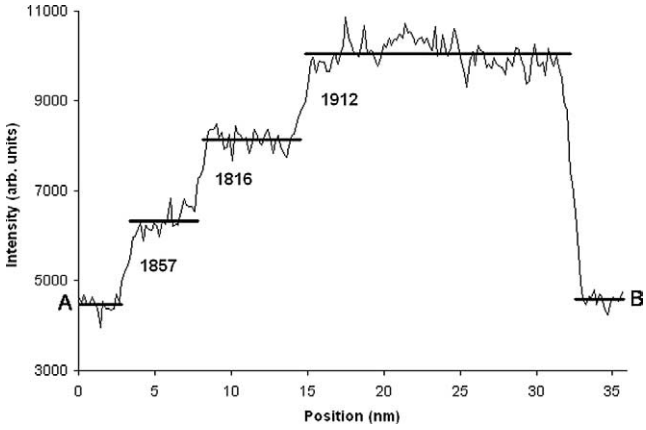

Fig. 9. Intensity line trace of the three-layer WS_2 nanocluster of Fig. 8. The trace follows the line A to B in Fig. 8 and the values for the step heights in the graph show an even increase in intensity when extra S–W–S layers are added.

fect of the gaseous environment can be made. It is interesting that the large spread in shapes exists even after sulfiding at 1073 K, a temperature that is much higher than employed in most studies. This again suggests that the nucleation and growth are very much influenced by the graphite support and quite large differences in morphology may even be observed for WS_2 nanoclusters on the same graphite sheet. It should finally be stressed that WS_2 may behave differently from MoS_2 and the relative stabilities of the different structures may be different. Thus a direct comparison with DFT and STM measurements for MoS_2 is not necessarily possible.

4. Conclusion

One of the difficulties with HRTEM studies of supported MoS_2 (WS_2) nanoclusters is the inability to obtain shape information since the nanoclusters are invisible when viewed with the *c* axis parallel to the electron beam. Thus, calculations regarding edge dispersion have been based on assumptions regarding the morphology. The present results show that HAADF-STEM may provide this important insight. In addition, this method readily allows a quantitative analysis since in contrast to HRTEM, all the metal sulfide nanoclusters are readily observed. Besides providing a much better estimate of the overall edge dispersion, many more details regarding the concentration of other types of sites, such as, e.g., corner sites, may be obtained. This, in combination with catalytic measurements, could provide us with a better understanding of the active sites in supported MoS_2 (WS_2) catalysts. We are currently exploring the possibilities of determining the concentrations of the individual Mo and S edges by introducing suitable titrants before the HAADF-STEM measurements. The fact that we can produce predominantly monolayer structures may allow us to unravel the catalytic influence of the different types of edges without having to consider, for example, steric effects caused by having several different multilayer structures present in the same catalyst.

References

[1] R. Prins, V.H.J. de Beer, G.A. Somorjai, Catal. Rev. Rev.-Sci. Eng. 31 (1989) 1.
[2] H. Topsøe, B.S. Clausen, F.E. Massoth, in: J.R. Anderson, M. Boudart (Eds.), Hydrotreating Catalysis, Science and Technology, vol. 11, Springer, Berlin, 1996.
[3] T. Kabe, A. Ishihara, W. Qian, Hydrodesulfurization and Hydrodegenation, Chemistry and Engineering, Wiley–VCH, Kodanska, 1999.
[4] M.V. Landau, Catal. Today 36 (1997) 393.
[5] D.D. Whitehurst, T. Isoda, I. Mochida, Adv. Catal. 42 (1998) 345.
[6] K.G. Knudsen, B.C. Cooper, H. Topsøe, Appl. Catal. A 189 (1999) 205.
[7] C. Song, Catal. Today 86 (2003) 211.
[8] B.S. Clausen, H. Topsøe, R. Candia, J. Villadsen, B. Lengeler, J. Als-Nielsen, F. Christensen, J. Phys. Chem. 85 (1982) 3868.
[9] B.S. Clausen, H. Topsøe, R. Candia, B. Lengeler, in: K.O. Hodgson, et al. (Eds.), EXAFS and Near Edge Structure III, Springer, Berlin, 1984, p. 181.
[10] T.G. Parham, R.P. Merrill, J. Catal. 85 (1984) 295.
[11] H. Topsøe, B.S. Clausen, Appl. Catal. 25 (1986) 273.
[12] S.M.A.M. Bouwens, R. Prins, V.H.J. de Beer, D.C. Koningsberger, J. Phys. Chem. 94 (1990) 3711.
[13] Y. Okamoto, Catal. Today 39 (1997) 45.
[14] C. Calaix, N. Matsubayashi, C. Geantet, Y. Yoshimura, H. Shimada, A. Nishijima, M. Lacroix, M. Breysse, J. Catal. 174 (1998) 130.
[15] T. Shido, R. Prins, J. Phys. Chem. B 102 (1998) 8426.
[16] G. Plazenet, S. Cristol, J.-F. Paul, E. Payen, J. Lynch, Phys. Chem. Chem. Phys. 3 (2001) 246.
[17] N.-Y. Topsøe, J. Catal. 64 (1980) 235.
[18] J. Grimblot, P. Dufresne, L. Gengembre, J.-P. Bonelle, Soc. Chim. Belg. 90 (1981) 1311.
[19] J.V. Sanders, Phys. Scr. 14 (1978/79) 141.
[20] J.M. Thomas, G.R. Millward, L.A. Bursell, Philos. Trans. R. Soc. A 300 (1981) 43.
[21] H. Topsøe, in: J.P. Bonelle, et al. (Eds.), Surface Properties and Catalysis by Non-Metals, Reidel, Dordrecht, 1983, p. 329.
[22] R. Candia, O. Sørensen, J. Villadsen, N.-Y. Topsøe, B.S. Clausen, H. Topsøe, Bull. Soc. Chim. Belg. 93 (1984) 763.
[23] F. Delannay, Appl. Catal. 16 (1985) 135.
[24] T.F. Hayden, J.A. Dumesic, J. Catal. 103 (1987) 366.
[25] J. Ramirez, S. Fuentes, G. Diaz, M. Vrinat, M. Breysse, M. Lacroix, Appl. Catal. 52 (1989) 211.
[26] E. Payen, S. Kasztelaan, S. Houssenbay, R. Szymanski, J. Grimblot, J. Phys. Chem. 93 (1989) 6501.
[27] R.R. Chianelli, M. Daage, in: M.L. Occelli, R.G. Anthony (Eds.), Hydrotreating Catalysts—Preparation Characterization and Performance, Elsevier, Amsterdam, 1989, p. 120.
[28] J. Lindner, A. Sachdev, J. Schwank, M. Villa-Garcia, J. Catal. 137 (1992) 333.
[29] S. Srinivasan, A.K. Datye, C.H.F. Peden, J. Catal. 137 (1992) 513.
[30] S. Eijsbouts, J.J.L. Heinerman, H.J.W. Elzerman, Appl. Catal. A 105 (1993) 53.
[31] P.L. Hansen, H. Topsøe, J.O. Malm, in: Proc. 13th Int. Conf. on Electron Microscopy, Paris, vol. 2B, 1994, p. 1077.
[32] R.M. Stockmann, H.W. Zandbergen, A.D. van Langeveld, J.A. Moulijn, J. Mol. Catal. A 102 (1995) 147.
[33] S. Eijsbouts, Appl. Catal. A 158 (1997) 53.
[34] P. Da Silva, N. Marchal, V. Harlé, T. Cseri, S. Kasztelaan, ACS Pet., Preprint 1998, p. 20.
[35] Y. Sakushita, T. Yoneda, J. Catal. 185 (1999) 487.
[36] Y. Araki, K. Honna, H. Shimada, J. Catal. 207 (2002) 361.
[37] H.R. Reinhoudt, A.D. van Langeveld, P.J. Kooyman, R.M. Stockmann, R. Prins, H.W. Zandbergen, J.A. Moulijn, J. Catal. 179 (1998) 443.
[38] P.J. Kooyman, E.J.M. Hensen, A.M. de Jong, J.W. Niemantsverdriet, J.A.R. van Veen, Catal. Lett. 74 (2001) 49.

[39] S. Helveg, J.V. Lauritsen, E. Lægsgaard, I. Stensgaard, J.K. Nørskov, B.S. Clausen, H. Topsøe, F. Besenbacher, Phys. Rev. Lett. 84 (2000) 951.
[40] J.V. Lauritsen, M.V. Bollinger, E. Lægsgaard, K.W. Jacobsen, J.K. Nørskov, B.S. Clausen, H. Topsøe, F. Besenbacher, J. Catal. 221 (2004) 510.
[41] A.V. Crewe, J.P. Wall, J.P. Langmore, Science 168 (1970) 1138.
[42] M.M. Treacy, A. Howie, S.J. Pennycook, Inst. Phys. Conf. Ser. 52 (1980) 261.
[43] J.M. Thomas, O. Terasaki, Top. Catal. 21 (2002) 155.
[44] A.K. Datye, J. Catal. 216 (2003) 144.
[45] S. Hillyard, J. Silcox, Ultramicroscopy 58 (1995) 6.
[46] E.M. James, N.D. Browning, Ultramicroscopy 78 (1999) 125.
[47] L.S. Byskov, J.K. Nørskov, B.S. Clausen, H. Topsøe, J. Catal. 187 (1999) 109.
[48] L.S. Byskov, J.K. Nørskov, B.S. Clausen, H. Topsøe, Catal. Lett. 64 (2000) 95.
[49] P. Raybaud, J.H. Hafner, G. Kresse, S. Kasztelaan, H. Toulhoat, J. Catal. 189 (2000) 129.
[50] S. Cristol, J.-F. Paul, E. Payen, D. Bougeard, S. Clémendot, F. Hutschka, J. Phys. Chem. B 104 (2000) 11,220.
[51] V. Alexiev, R. Prins, T. Weber, Phys. Chem. Chem. Phys. 3 (2001) 5326.
[52] H. Schweiger, P. Raybaud, G. Kresse, H. Toulhoat, J. Catal. 207 (2002) 76.
[53] M.V. Bollinger, K.W. Jacobsen, J.K. Nørskov, Phys. Rev. B 67 (2003) 085,410.